ASSEMBLY BIAS AND THE DYNAMICAL STRUCTURE OF DARK MATTER HALOS

Andreas Faltenbacher[1,2,3] and Simon D. M. White[1]
Draft version November 18, 2009

ABSTRACT

Based on the Millennium Simulation we examine assembly bias for the halo properties : shape, triaxiality, concentration, spin, shape of the velocity ellipsoid and velocity anisotropy. For consistency we determine all these properties using the same set of particles, namely all gravitationally self–bound particles belonging to the most massive sub–structure of a given friends–of–friends halo. We confirm that near–spherical and high–spin halos show enhanced clustering. The opposite is true for strongly aspherical and low–spin halos. Further, below the typical collapse mass, M_*, more concentrated halos show stronger clustering whereas less concentrated halos are less clustered which is reversed for masses above M_*. Going beyond earlier work we show that: (1) oblate halos are more strongly clustered than prolate ones; (2) the dependence of clustering on the shape of the velocity ellipsoid coincides with that of the real–space shape, although the signal is stronger; (3) halos with weak velocity anisotropy are more clustered, whereas radially anisotropic halos are more weakly clustered; (4) for all highly clustered subsets we find systematically less radially biased velocity anisotropy profiles. These findings indicate that the velocity structure of halos is tightly correlated with environment.

Subject headings: cosmology: theory – cosmology : dark matter – methods: N-body simulations

1. INTRODUCTION

The dependence of halo clustering on a second parameter in addition to mass is now generally referred to as assembly bias. Analytic models predict the clustering of halos to depend on their mass alone (Kaiser 1984; Cole & Kaiser 1989; Mo & White 1996). However, Gao et al. (2005) and various subsequent studies showed that clustering also depends on other halo properties like formation time, concentration, substructure content, spin and shape (Harker et al. 2006; Wechsler et al. 2006; Bett et al. 2007; Gao & White 2007; Jing et al. 2007; Macciò et al. 2007; Wetzel et al. 2007; Angulo et al. 2008).

It soon became clear that the dependency of clustering on the various parameters does not simply follow from the relation among those parameters. Here are two examples: (1) Earlier formed halos have higher concentrations (e.g., Navarro et al. 1997; Wechsler et al. 2002; Neto et al. 2007) nevertheless the dependence of clustering on formation time and concentration show different behavior (cf., Jing et al. 2007). (2) As discussed in Bett et al. (2007) there is a weak correlation between spin and shape, more spherical halos show on average a slightly lower spin parameter. However, the bias behavior is opposite to what one would naively derive from this correlation. The most nearly spherical halos and the halos with highest spins are clustered above average (see also, Gao & White 2007). These examples suggest that the ranking according to any given parameter, like concentration, spin or shape cannot be converted in any simple way to the approximate ranking according to another parameter. In this context Croton et al. (2007)

speculated (but did not demonstrate) that there may be a more fundamental parameter capable of uniquely predicting halo clustering.

Simple implementations of extended Press-Schechter and excursion set models (Press & Schechter 1974; Bond et al. 1991; Lacey & Cole 1993) commonly used to estimate halo statistics do not predict a dependence of formation time on environment. However, using a mass filter in configuration space rather than in k-space Zentner (2007) demonstrated that halos in denser environments do form later independent of halo mass. At the high mass end this agrees with findings from N-body simulations (e.g., Wechsler et al. 2002; Jing et al. 2007) but is opposite to the behavior observed at the low mass end (e.g., Gao et al. 2005).

Dalal et al. (2008) argued that for high halo masses assembly bias is expected from the statistics of the peaks of Gaussian random fluctuations and at low masses it arises from a subpopulation of low-mass halos whose mass accretion has ceased. It is unclear whether whether other aspects of assembly bias can be explained in this way.

Several other studies have investigated the dependence of halo formation times or, similarly, merger rates on environment (e.g., Gottlöber et al. 2001, 2002; Sheth & Tormen 2004; Fakhouri & Ma 2009b,a; Hahn et al. 2009). Although, slightly different density estimators, like over density in a sphere or mark correlation functions, are employed it is generally agreed upon that halos less massive than $\sim 10^{13} \, h^{-1}M_\odot$ which reside in high density regions form earlier compared to those with equal mass but located in less dens regions.

Most of the previous studies examined the impact of the assembly bias on galaxy clustering statistics. This is not the prime focus of this work. We are mainly concerned about the interplay between clustering and the dynamical structure of halos. To describe the dynamical structure of halos we use a variety of parameters, namely: the mean shape, the mean triaxiality, the spin, the non-dimensionlized total velocity dispersion (a mea-

[1] Max Planck Institut für Astrophysik, Karl-Schwarzschild-Str. 1, 85741 Garching, Germany
[2] MPA/SHAO Joint Center for Astrophysical Cosmology at Shanghai Astronomical Observatory, Nandan Road 80, Shanghai 200030, China
[3] Physics Department, University of the Western Cape, Cape Town 7535, South Africa

sure of concentration), the shape of the global velocity dispersion tensor, and the mean radial/tangential velocity anisotropy. We also explore whether subsets of halos which show assembly bias share any common property. The most obvious we find is the behavior of velocity anisotropy. On average, all highly clustered subsets appear to have less radially biased internal motions. The opposite holds for less clustered subsets.

2. METHODOLOGY

2.1. Simulation

The Millennium Simulation (Springel et al. 2005) adopted concordance values for the parameters of a flat Λ cold dark matter (ΛCDM) cosmological model, $\Omega_{\rm dm} = 0.205$ and $\Omega_{\rm b} = 0.045$ for the current densities in CDM and baryons, $h = 0.73$ for the present dimensionless value of the Hubble constant, $\sigma_8 = 0.9$ for the rms linear mass fluctuation in a sphere of radius $8\,h^{-1}$Mpc extrapolated to $z = 0$, and $n = 1$ for the slope of the primordial fluctuation spectrum. The simulation followed 2160^3 dark matter particles from $z = 127$ to the present day within a cubic region $500\,h^{-1}$Mpc on a side resulting in individual particle masses of $8.6 \times 10^8\,h^{-1}{\rm M}_\odot$. The gravitational force had a Plummer-equivalent comoving softening of $5\,h^{-1}$kpc. The Tree-PM N-body code GADGET2 (Springel 2005) was used to carry out the simulation and the full data were stored 64 times spaced approximately equally in the logarithm of the expansion factor.

2.2. Halo sample and properties

The halos are found by a two-step procedure. In the first step all collapsed halos with at least 20 particles are identified using a friends-of-friends (FoF) group-finder with linking parameter b = 0.2. These objects will be referred to as FoF-halos. Then post-processing with the substructure algorithm SUBFIND (Springel et al. 2001) subdivides each FoF-halo into a set of self-bound subhalos. Here we only consider the most massive sub-halo within each FoF–halo which on average comprises $\sim 80\%$ of the total mass of the FoF–halo. We refer to these subhalos simply as halos. As is common practice we chose the position of the most bound particle of that sub–halo as center of the halo. All halo properties are consistently computed based on particles assigned to that (most massive sub-) halo. That way possible confusion due properties which are computed based on different halo definitions can be excluded. For instance, commonly the spin parameter is determined withn a spherical volume whereas the shape is based on all particles associated with the FoF–halo. In this study, however, both quantities are computed based on the same set of particles.

As is standard, the shape, $s = a/c$, the triaxiality, $T = (a^2 - b^2)/(a^2 - c^2)$, and the shape of the velocity ellipsoids, $s_{\rm v} = a_{\rm v}/c_{\rm v}$ are computed based on the eigenvalues $(a_{(\rm v)} > b_{(\rm v)} > c_{(\rm v)})$ of the second moments of the spatial and velocity distributions of all halo particles. The velocity anisotropy parameter is given by $\beta = 1 - 0.5\,\sigma_{\rm t}^2/\sigma_{\rm r}^2$, where $\sigma_{\rm r}$ and $\sigma_{\rm t}$ are the radial and tangential velocity dispersion based on all halo particles. Since the conventional determination of the spin parameter and the concentration is based on the particle content within a sphere and not on self-bound particles we introduce slightly different quantities to replace them. The

spin, l, is computed as the absolute value of the total angular momentum multiplied by the Hubble constant H to the one third power and divided by the total mass M to the power 5/3. This is closely related to the formula given in Bullock et al. (2001). As quantity measuring concentration, we use $C = \sigma/(HM)^{1/3}$ where σ is the total velocity dispersion of the halo. Concentration and σ are positively correlated, i.e. high σ values correspond to high concentrations and vice versa. The powers of mass in the denominators of l and C are chosen to compensate for the intrinsic mass dependence of these quantities.

2.3. Determining the bias factor

The determination of the bias factor, b, follows the approach given in Gao & White (2007). It is computed as the relative normalization factor which minimizes the mean square of the difference $\log \xi_{\rm hm} - \log b\xi_{\rm mm}$ for four equal width bins in $\log r$ spanning the comoving separation range $6 < r < 20\,h^{-1}$Mpc. Here, $\xi_{\rm hm}$ is the halo mass cross-correlation function and $\xi_{\rm mm}$ is the mass autocorrelation function. Compared to estimators based on the halo autocorrelation function this estimator has highly improved noise characteristics because of the large number of dark matter particles available. As suggested by standard halo bias models (Mo & White 1996) and verified numerically by Gao & White (2007) this approach is equivalent to estimators based on halo autocorrelation functions. The large-scale bias depends on mass and redshift through the equivalent peak height $\nu(M, z) = \delta_c(z)/\sigma(M, z)$, where $\sigma(M, z)$ is the rms linear overdensity within a sphere which contains the mass M in the mean, and $\delta_c(z)$ is the linear overdensity threshold for collapse at redshift z. The typical collapse mass, M_*, corresponds to $\nu = 1$. We will use the equivalent peak height to seamlessly combine results derived at redshifts $z = 0, 1, 2$ and 3.

3. RESULTS

3.1. Assembly bias based on consistent halo properties

Fig. 1 shows the assembly bias based on halo properties as defined in $\S$ 2.2. Symbols (squares, diamonds, triangles) display bias factors for all halos. Solid and dashed lines give the bias based on the upper and lower 20 % tiles of the distributions of each specific property as indicated by labels in the lower right corners. We use solid red lines for the more strongly biased tail and dashed blue lines for the more weakly biased tail. These line styles are adopted in Fig 2 to ease comparison. Given that C and l correspond closely to conventional concentration and spin we confirm the results reported in previous work. However, with triaxiality, T, shape of the velocity ellipsoid, $s_{\rm v}$, and the velocity anisotropy, β, we add three more properties which show significant assembly bias.

The displayed dependency of bias on shape, s, reproduces the results by Bett et al. (2007). For all masses, more nearly spherical halos are clustered above, and strongly aspherical halos below average. The behavior of the triaxiality, T, indicates that prolate halos are clustered below average and oblate halos are more strongly clustered than average. The results for the scaled velocity dispersion, C, which here replaces the conventional concentration, indicate that for $\nu \lesssim 1$ high concentration halos are more and low concentration halos are less
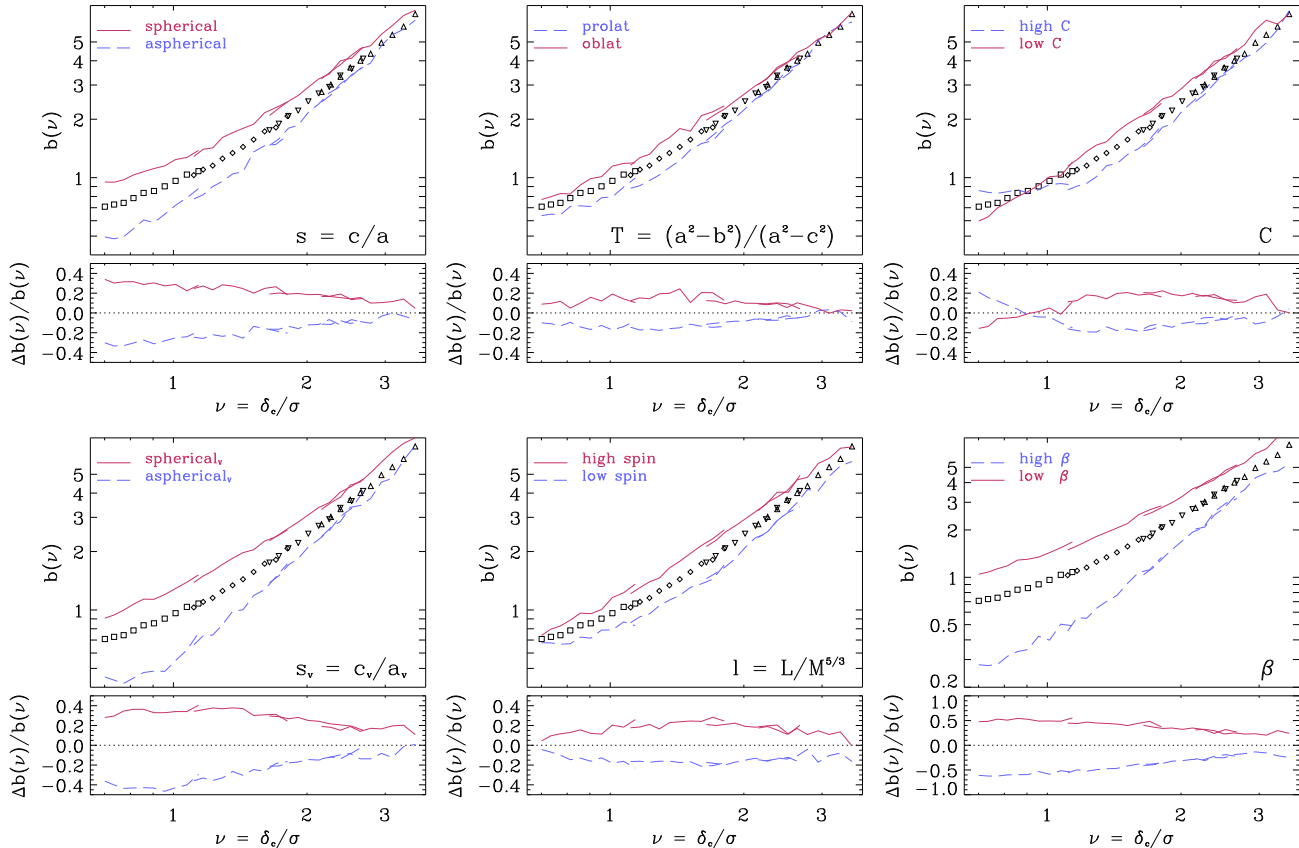
FIG. 1.— Bias factor as a function of halo mass and halo properties. Halo mass is given parametrically through the equivalent peak height $\nu = \delta_c/\sigma$. The additional properties in the six panels are: shape (s), Triaxiality (T) , concentration (C), shape of the velocity ellipsoid (s_v), the spin (L) and the velocity anisotropy (β). Symbols are bias factors defined for all haloes in a given mass bin. The various shapes (squares, diamonds, two kinds of triangles) indicate the redshifts (0,1,2,3) of the snapshots used to determine them. The same redshifts are used for the computation of the solid curves which are bias factors for haloes in the lower and upper 20 % tails of the distributions of the particular property concerned.

clustered. This behavior reverses sign for $\nu \gtrsim 1$. The same trends have been reported in Wechsler et al. (2006), Gao & White (2007), Jing et al. (2007) and Wetzel et al. (2007). The particularly good agreement with Fig.2 in Jing et al. (2007) based on the conventional concentration increases confidence that C can represent concentration in the context of assembly bias studies. The shape of the velocity ellipsoid, s_v, behaves similarly to the shape of the spatial distribution, s. The dependence of clustering on spin, l, is comparable to the results in Bett et al. (2007) and Gao & White (2007). Finally, halos with low velocity anisotropy, β, are more clustered and the opposite holds for halos with strongly radially biased velocities. The signal based on β is the most pronounced among all shown here indicating that velocity related quantities are tightly correlated with the clustering strength.

We also obtained results for the dependence of clustering on formation time (not shown) as examined in Gao et al. (2005). As formation time for their *fof-halos* they used the time when half the final was acquired. For a variety of reasons we here restrict ourselves to self–bound main subhalos which are simpler and better defined objects. Thus we computed the formation times in the same way as Gao et al. (2005) except that we use main subhalos. It turned out that the effect is qualitatively similar to that found earlier but is *much* weaker. We find only a ~ 10 per cent increase of the bias factor for early formed halos at masses corresponding to $\nu \lesssim 1$. Different factors like the orbital parameters or the concentrations of the merging systems imply a certain stochasticity of the sub-halo masses which propagates into the determination of the formation times and reduces the assembly bias signal. Li et al. (2008) noted that the definition of the formation time has a substantial impact on the strength of the assembly bias, confirming that the change from fof- to sub-halo accretion histories is responsible for the reduction of the assembly bias signal.

3.2. *Do highly clustered halo subsets share similar properties?*

To find out whether highly clustered halo subsets share similar properties we compute stacked profiles of the halos belonging the 20 % tail subsets of a given property, and compare them with the stacked profiles of all halos. We examine the difference in density, velocity dispersion, phase space density and velocity anisotropy profiles. Density and velocity dispersion profiles show no unique trend with the bias behavior.

The average phase space density profiles determined by ρ/σ^3 indicate that more strongly clustered subsets, solid red lines in Fig. 1, tend to lie above the average profiles based on all halos in a given mass bin. However, for some properties, like spin and velocity anisotropy, the differences are small and dependent on radius.
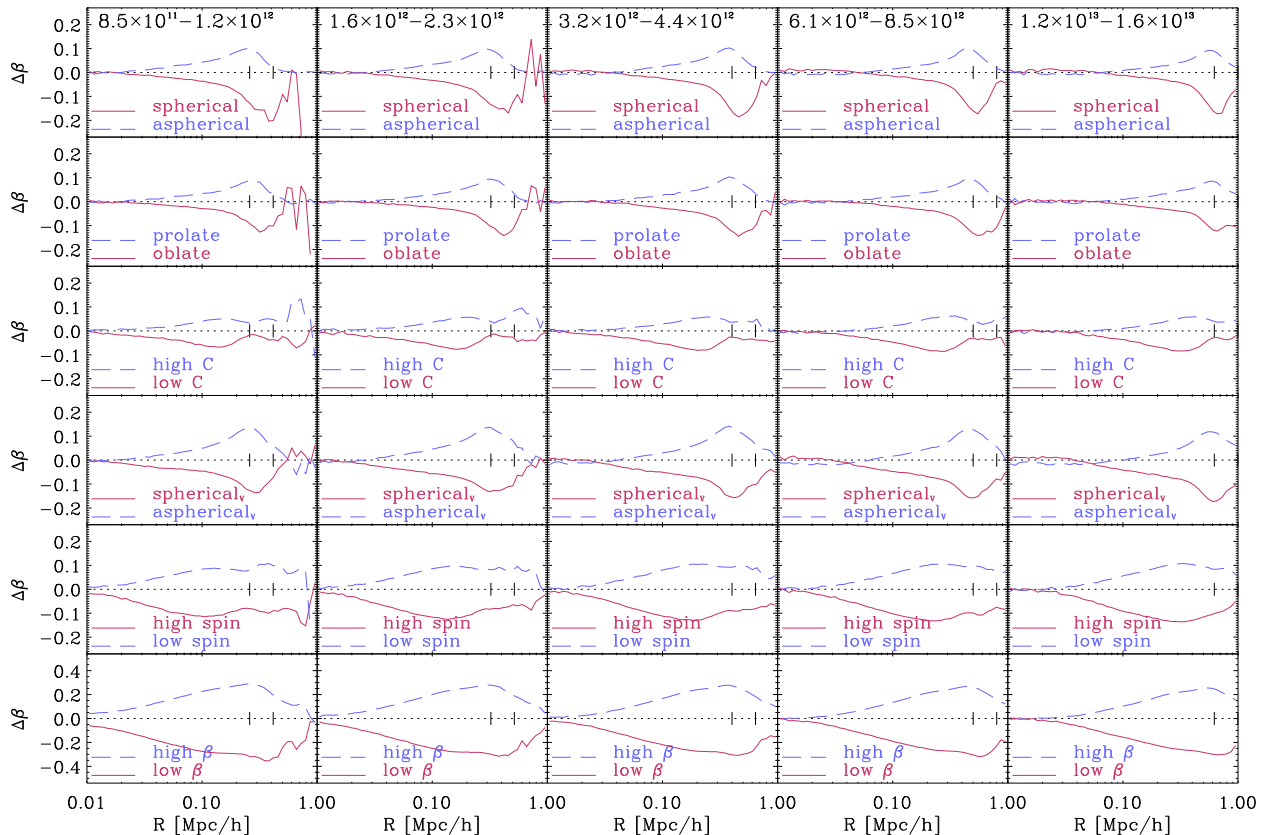
FIG. 2.— Difference between the average velocity anisotropy profiles, $\Delta\beta$, of halos in the 20 per cent tails of the according distribution and all halos at a given mass. The same halo properties are used as in Fig. 1. From top to bottom they are: shape, triaxiality, scaled velocity dispersion, shape of velocity ellipsoid, spin and velocity anisotropy. Columns correspond to every second symbol for $\nu \lesssim 1$ in Fig. 1. The two short vertical lines indicate the averages of the radii including a mean density of 200 times the critical and 200 times the cosmic mean density, respectively. The averages are based on all halos in a given mass bin. Averages based on halos in the tails of the distributions show only marginal differences. In the rightmost column the outer marks exceed the plot range. Signals beyond the marks are dominated by effects of the boundaries of our halos.

Motivated by studies of Hansen et al. (2006) and Schmidt et al. (2008) we also probe the behavior for phase space densities computed as ρ/σ_r^3, where σ_r denotes the radial velocity dispersion. For masses larger than M_* the average phase space profiles of subsets which show stronger clustering (solid red lines in Fig. 1) systematically lie above the average profiles of all halos. Profiles based on less clustered subsets fall below the average profiles based on all halos in a given mass bin. However, for halo masses below M_* the reversal of sign seen in concentration (velocity dispersion) is not reproduced. Schmidt et al. (2008) argued that there is no empirical justification (but see also Dehnen & McLaughlin 2005) for the particular definition of phase space density used here, and we find that changing the exponent of the velocity dispersion definitely has an impact on the correlation between clustering and phase space profiles. Due to such uncertainties we leave the discussion at this point. Nevertheless, we note there is a systematic trend for more clustered halos to have higher phase space densities.

In contrast to the phase space profiles the velocity anisotropy profiles, $\beta(r) = 1 - 0.5\sigma_r^2(r)/\sigma_t^2(r)$, are unambiguously defined ($\sigma_r(r)$ and $\sigma_t(r)$ denotes the radial and the tangential velocity dispersions averaged in spherical shells). Fig. 2 shows the difference, $\Delta\beta$, between the stacked velocity anisotropy profiles of all halos and the halos belonging to 20 % tails of the distribution of a given

property. These properties are, from top to bottom: shape, triaxiality, scaled velocity dispersion, shape of the velocity ellipsoid, spin and total velocity anisotropy. The columns show various mass bins corresponding to every second mass bin with $\nu \lesssim 1$ in Fig 1. The comparison with Fig. 1 indicates that more clustered subsets (solid red lines) show on average lower β profiles. The opposite holds for the less clustered subsets (dashed blue lines). For the scaled velocity dispersion, C, the difference is strongly reduced, however the reversal of the sign as apparent in Fig. 1 is not explicitly reproduced. But apart from that, there is a clear correlation between clustering behavior and velocity anisotropy.

One possible explanation for the more nearly isotropic global velocity distribution of more clustered halos is that the impact parameters of the merging sub-halos are larger due to gravitational deflections short time before accretion. Fakhouri & Ma (2009a) have shown that mergers are the dominant mode of accretion in high density regions thus they presumably determine the velocity structure of these halos. On the other side in lower density regions the gravitational field is dominated by the halo itself and accretion occurs in a more radial fashion leaving the observed imprint on the velocity structure of the halo.

4. CONCLUSION

Taking advantage of the large volume and the superior resolution of the Millennium Simulation we reassess assembly bias for various halo properties. We conclude with a recapitulation of the main results:

1) Based on consistent determinations of various halo properties, like shape, spin and concentration, we confirm the results reported in previous studies. More nearly spherical and high–spin halos are clustered above and aspherical and low–spin below average. Below the typical collapse mass, M_*, more concentrated halos show stronger clustering whereas less concentrated halos are less clustered. This reverses for masses above M_*. The clustering cannot simply be explained by the relations among the properties.

2) To the halo properties which have already been shown to correlate with clustering behavior, we have added the triaxiality, the shape of the global velocity ellipsoid and the velocity anisotropy parameter. Oblate halos, halos with a more nearly isotropic global velocity distribution and halos with weak velocity anisotropy are more clustered than average. Contrary properties reduce clustering. Very prominent signals are found for the velocity–related properties, indicating that halo velocity structure is tightly correlated with the clustering behavior.

3) We also showed that independent of the halo property (shape, triaxiality, spin, concentration) the velocity anisotropy profile of the more clustered subsets lies systematically below the average profile, whereas less clustered subsets show profiles, indicating more radially biased internal motions.

Our findings show that the internal velocity structure of halos is strongly influenced by environment. Halos are not "universal" and their internal properties (the deviations from universality) are related in complex ways to their environment.

REFERENCES

Angulo, R. E., Baugh, C. M., & Lacey, C. G. 2008, MNRAS, 387, 921

Bett, P., Eke, V., Frenk, C. S., Jenkins, A., Helly, J., & Navarro, J. 2007, MNRAS, 376, 215

Bond, J. R., Cole, S., Efstathiou, G., & Kaiser, N. 1991, ApJ, 379, 440

Bullock, J. S., Dekel, A., Kolatt, T. S., Kravtsov, A. V., Klypin, A. A., Porciani, C., & Primack, J. R. 2001, ApJ, 555, 240

Cole, S. & Kaiser, N. 1989, MNRAS, 237, 1127

Croton, D. J., Gao, L., & White, S. D. M. 2007, MNRAS, 374, 1303

Dalal, N., White, M., Bond, J. R., & Shirokov, A. 2008, ApJ, 687, 12

Dehnen, W. & McLaughlin, D. E. 2005, MNRAS, 363, 1057

Fakhouri, O. & Ma, C. 2009a, ArXiv e-prints

—. 2009b, MNRAS, 394, 1825

Gao, L., Springel, V., & White, S. D. M. 2005, MNRAS, 363, L66

Gao, L. & White, S. D. M. 2007, MNRAS, 377, L5

Gottlöber, S., Kerscher, M., Kravtsov, A. V., Faltenbacher, A., Klypin, A., & Müller, V. 2002, A&A, 387, 778

Gottlöber, S., Klypin, A., & Kravtsov, A. V. 2001, ApJ, 546, 223

Hahn, O., Porciani, C., Dekel, A., & Carollo, C. M. 2009, MNRAS, 398, 1742

Hansen, S. H., Moore, B., Zemp, M., & Stadel, J. 2006, Journal of Cosmology and Astro-Particle Physics, 1, 14

Harker, G., Cole, S., Helly, J., Frenk, C., & Jenkins, A. 2006, MNRAS, 367, 1039

Jing, Y. P., Suto, Y., & Mo, H. J. 2007, ApJ, 657, 664

Kaiser, N. 1984, ApJ, 284, L9

Lacey, C. & Cole, S. 1993, MNRAS, 262, 627

Li, Y., Mo, H. J., & Gao, L. 2008, MNRAS, 389, 1419

Macciò, A. V., Dutton, A. A., van den Bosch, F. C., Moore, B., Potter, D., & Stadel, J. 2007, MNRAS, 378, 55

Mo, H. J. & White, S. D. M. 1996, MNRAS, 282, 347

Navarro, J. F., Frenk, C. S., & White, S. D. M. 1997, ApJ, 490, 493

Neto, A. F., Gao, L., Bett, P., Cole, S., Navarro, J. F., Frenk, C. S., White, S. D. M., Springel, V., & et al., 2007, MNRAS, 381, 1450

Press, W. H. & Schechter, P. 1974, ApJ, 187, 425

Schmidt, K. B., Hansen, S. H., & Macciò, A. V. 2008, ApJ, 689, L33

Sheth, R. K. & Tormen, G. 2004, MNRAS, 350, 1385

Springel, V. 2005, MNRAS, 364, 1105

Springel, V., White, S. D. M., Jenkins, A., Frenk, C. S., Yoshida, N., Gao, L., Navarro, J., Thacker, R., & et al., 2005, Nature, 435, 629

Springel, V., White, S. D. M., Tormen, G., & Kauffmann, G. 2001, MNRAS, 328, 726

Wechsler, R. H., Bullock, J. S., Primack, J. R., Kravtsov, A. V., & Dekel, A. 2002, ApJ, 568, 52

Wechsler, R. H., Zentner, A. R., Bullock, J. S., Kravtsov, A. V., & Allgood, B. 2006, ApJ, 652, 71

Wetzel, A. R., Cohn, J. D., White, M., Holz, D. E., & Warren, M. S. 2007, ApJ, 656, 139

Zentner, A. R. 2007, International Journal of Modern Physics D, 16, 763